Heliyon 8 (2022) e10430

Contents lists available at ScienceDirect

Heliyon

journal homepage: www.cell.com/heliyon

Research article

Change in Salinity of Indonesian Upper Water in the Southeastern Indian Ocean during Argo Period

Mochamad Riza Iskandar [a,*], Toshio Suga [b]

[a] Research Center for Oceanography, National Research and Innovation Agency, Pasir Putih 1, Ancol Timur, Jakarta 14430, Indonesia
[b] Department of Geophysics, Tohoku University, Sendai 980-8578, Japan

HIGHLIGHTS

- Changes in the Indonesian Upper Water (IUW) salinity are observed between 2004-2020 in the Indian Ocean.
- The IUW has experienced a basin-scale freshening from 2004 to 2013, and the opposite change appears from 2014 to 2020.
- Oceanic-atmospheric mechanisms in the Maritime Continent shape the salinity changes in the southeastern Indian Ocean.

GRAPHICAL ABSTRACT

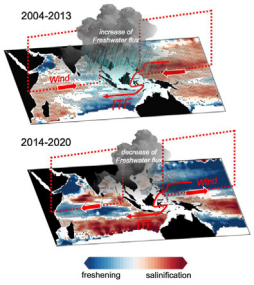

ARTICLE INFO

Keywords:
Indonesian upper water
Southeastern Indian ocean
Salinity
Indonesian throughflow

ABSTRACT

The change in salinity of Indonesian Upper Water (IUW) in the Indian Ocean has been examined during 2004–2020 based on the Argo product. Monthly salinity fields reveal a contrast of IUW salinity changes between two time periods (2004–2013 and 2014–2020) in the outflow of Indonesian Throughflow (ITF) in the Indian Ocean. Freshening of IUW has been observed in the Indian Ocean from 2004-2013 on a basin scale. The opposite changes appear from 2014-2020, when IUW shows a general increase in salinity. The present study shows that oceanic-atmospheric processes in the Maritime Continent influence the changes in the IUW salinity in the southeastern Indian Ocean. The salinity changes are connected to the alteration of the freshwater flux in the Maritime Continent. The ITF enhances subsequent salinity transport into the southeastern Indian Ocean. Zonal atmospheric circulation strength in the tropical region is linked to the shift of the large freshwater flux in the Maritime Continent.

1. Introduction

The Indonesian Sea is a unique region of the world, not only because of the only low-latitude passage in the world's ocean but also because of its oceanic and atmospheric characteristics (Ffield and Gordon, 1996; Fieux et al., 1994; Gordon, 1986; Gordon and Fine, 1996; Ilahude and Gordon, 1996; Koch-Larrouy et al., 2008; Sprintall and Revelard, 2014; Tillinger and Gordon, 2009; Vranes et al., 2002). The Indonesian Seas provide an oceanic passage connecting the tropical Pacific and the Indian Ocean, known as the Indonesian Throughflow (ITF) (Gordon, 1986). This passage is one part of the global thermohaline circulation at low-latitudes. It plays an essential role in the transfer of heat and freshwater, affecting the state and air-sea exchange of the Pacific and Indian Oceans that modulates climate variability on different time scales

* Corresponding author.
E-mail address: mochamad.riza.iskandar@brin.go.id (M.R. Iskandar).

https://doi.org/10.1016/j.heliyon.2022.e10430
Received 26 December 2021; Received in revised form 31 May 2022; Accepted 18 August 2022

(Hu et al., 2015; Kida and Richards, 2009; Lee et al., 2015; Potemra and Schneider, 2007; Sprintall et al., 2014; Sprintall and Revelard, 2014).

The gaps between New Guinea and the Philippines are the primary portals providing an interoceanic route through the Indonesian seas (Gordon, 1986, 2005; Li et al., 2021; Sprintall et al., 2014). The central inflow passage for the ITF is the Makassar Strait which consists mainly of North Pacific thermocline and intermediate water (western route, Figure 1a) (Gordon and Fine, 1996). Waters from the South Pacific enter through the passages that connect to the Halmahera Sea (eastern route, Figure 1a) (Gordon, 2005). They flow through Lifamatola Strait, where transport volume is estimated at 2.4–2.5 Sv, mainly near the bottom (van Aken et al., 2009). A recent study found that the Maluku Sea transports Antarctic Intermediate Water (AAIW) into Lifamatola Passage above the bottom overflow (Yuan et al., 2022). Secondary ITF portals provide a source of fresh water, which influences stratification in the ITF (South China Sea Throughflow, Figure 1a) (Gordon et al., 2012; Wang et al., 2006; Zeng et al., 2018). The water masses from the Indonesian Seas penetrate the Indian Ocean through gaps along Sumatra to Timor, such as Timor Passage, Ombai Strait, and Lombok Strait (Sprintall et al., 2009), Sunda Strait (Susanto et al., 2016), Savu Strait (Wang et al., 2020), and Alas Strait (Susanto et al., 2021).

During their stay in the Indonesian Seas, the incoming Pacific waters are modified to be a distinctive tropical stratification-having a relatively isohaline structure in the thermocline layer characterized by a very slight decrease in salinity with depth (Gordon, 2005; Koch-Larrouy et al., 2008; Sprintall et al., 2014; Talley and Sprintall, 2005). Isopycnal mixing is known to be responsible for the erosion of high-salinity water of the Pacific Ocean regulated by rigorous tidal mixing and local precipitation in the Indonesian Seas (Gordon et al., 2012; Gordon and Susanto, 2001; Hautala et al., 1996; Koch-Larrouy et al., 2010; Sprintall et al., 2014). The product of ITF water enters the Indian Ocean and flows westward by the South Equatorial Current (SEC), and then enters the Agulhas passage, moves to the Atlantic Ocean, joining the global circulation (Gordon, 1986; Talley and Sprintall, 2005). The throughflow waters crossing the Indian Ocean can be distinguished by their low salinity characteristics (Talley and Sprintall, 2005). There are two distinct water masses (Figures 1b, 1c and 1d), i.e., relatively fresh and warm water from the surface to the thermocline is referred to as Indonesian Upper Water (IUW), and fresh water in the deeper core of the throughflow is referred to as Indonesian Intermediate Water (IIW) that is independent of the salinity minimum of the AAIW in the Indian Ocean (Talley and Baringer, 1997; Talley and Sprintall, 2005).

The thermocline and intermediate waters contribute to global overturning circulation by ventilating the subtropical gyres in various ocean basins (Sloyan and Rintoul, 2001; Yao et al., 2017). Long-term changes in salinity have been examined using multiple data archives, which show that changes in salinity are intensified by the global hydrologic cycle (Boyer et al., 2005; Durack et al., 2012; Hosoda et al., 2009; Oka et al., 2017; Tesdal et al., 2018; Wong et al., 1999). Salinity shifts in the subtropical North Pacific gyre have been identified in several studies. Both isobaric and isopycnal freshening of the salinity minimum layers of the North Pacific Intermediate Water (NPIW) have been extensively observed and are attributed to changes in gyre circulation and surface freshening in the formation area (Lukas, 2001; Nakano et al., 2007; Nakanowatari et al., 2015; Wong et al., 1999, 2001).

An early study by Suga et al. (2000), using repeated data along 137°E during the 1967–1995 period, indicates that the NPTW area and salinity increased significantly with the 1976–1977 regime change. The long-term increase in the most saline part of the NPTW is related to excess evaporation over precipitation, Ekman pumping, and Pacific Decadal Oscillation (PDO) (Katsura et al., 2013; Oka et al., 2017, 2018). In the Southern Pacific, Kessler (1999) found that most of the interannual variation in salinity maximum of South Pacific Tropical Water (SPTW) tongue is related to oceanic advection and the El Niño-Southern Oscillation (ENSO). Based on the Argo float data, Zhang and Qu (2014) found a trend with the dipolar structure of SPTW during 2004–2012, which is related to the decadal variability of evaporation minus precipitation in the formation region. Long term increase in salinity in the upper 200 m of the subtropical South Pacific between 1955-1959 and 1994–1998 is also observed by Boyer et al. (2005). In addition, Wong et al. (2001) observed an increase in salinity between the 1960s and 1985–1994 that is related to the Pacific Decadal Oscillation (PDO).

Previous studies found that upper ocean salinity decreased in the western tropical Pacific and increased in the southeastern Indian Ocean

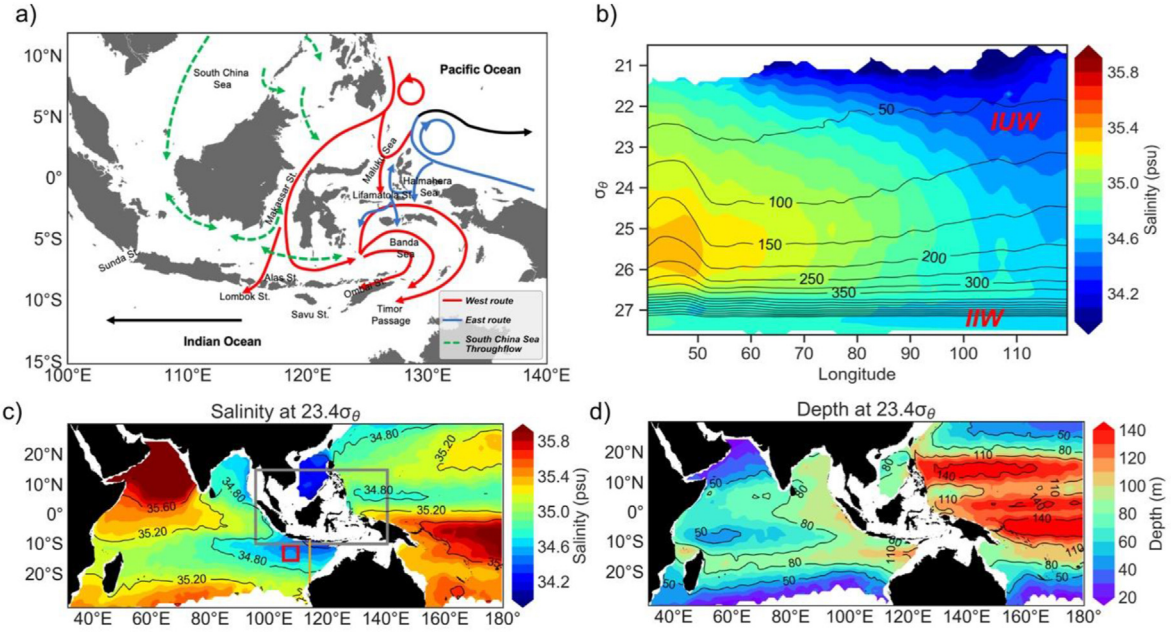

Figure 1. (a) Schematic of the Indonesian Throughflow (ITF), (b) mean salinity (2004–2020) along 12.5°S in the Indian Ocean on σ_θ coordinate, (c) mean salinity and (d) mean depth at $\sigma_\theta = 23.4$ kg m^{-3} (2004–2020). The red box in Figure (c) indicates the outflow region of Indonesian Throughflow (ITF), the grey box indicates the Maritime Continent, and the orange line indicates the section for calculation of the ITF. Contours in Figure (b) represent depth (m). Salinity data from Roemmich-Gilson Argo product.

from the 1950s to the late 1900s, which is related to the global hydrologic cycle and large-scale warming under the anthropogenic influence (Boyer et al., 2005; Cravatte et al., 2009; Durack et al., 2012; Hosoda et al., 2009; Skliris et al., 2016). In subsequent periods, Du et al. (2015) observed an opposite trend in sea surface salinity from the 1970s to the mid-1990s, with a contrasting trend pattern between an increase in the western tropical Pacific and a decrease in sea surface salinity in the southeastern Indian Ocean. They found that the trend appears to be related to increases in precipitation around the maritime continent and oceanic advection processes. The most recent study from Makarim et al. (2019) found that the southeastern Indian Ocean reveals rapid subsurface freshening and also warming since early 2000 that is consistent with the heat content changes. This occurs during the period of strengthening of ITF transport in association with the global warming hiatus during 2000–2009. It has also been reported that the negative phase of the Interdecadal Pacific Oscillation (IPO) is related to the decadal increase in precipitation over the Maritime Continent (Dong and Dai, 2015), which is also influenced by a long-term trend of the warming scenarios (Chou et al., 2009; Tan et al., 2015). These results imply that declining salinity in the southeastern Indian Ocean could reflect ocean-atmosphere processes on the Maritime Continent and could also relate to the driving force behind changes in the salinity of the throughflow water.

In contrast to the Pacific Ocean, little has been studied about salinity changes in the Indian Ocean. Specifically, there have been no detailed studies of the salinity of the IUW over the past decade, which are better captured by Argo data collected during 2004–2020. Therefore, this study focuses on the salinity shift of the IUW in the southeastern Indian Ocean during that period. The comparison identifies regions of salinity shift from 2004-2020, when Argo salinity measurements are available. The discussion on salinity shifts is observed through the monthly gridded of Roemmich-Gilson product (Roemmich and Gilson, 2009) in the potential density coordinate. Due to the scarcity of data in the Indonesian Seas, this study does not investigate the IUW in the formation area. Thus, we will focus and limit the explanation only to the southeastern Indian Ocean, where the IUW is mainly transported. Observed salinity changes are compared with reanalysis products of evaporation minus precipitation to elucidate the basic mechanisms underlying these changes. Furthermore, the possibility of a relationship between salinity changes on the Maritime Continent is investigated, i.e., the links to wind stress curl and the ITF transport. It is assumed that the ocean's feedback to the hydrological cycle surrounding the Maritime Continent can be detected remotely by investigating salinity shifts in the outflow of the ITF. The data and methodology are presented in the next section, the description of the change in water masses in the outflow of the ITF and its possible mechanisms is given in the Results and Discussion section, and finally, a summary of the results of the present study is given in the Conclusion.

2. Data and method

2.1. Data

2.1.1. Argo temperature and salinity

The primary data used in present study are the monthly gridded salinity and temperature from the Roemmich-Gilson (RG) Argo climatology (Roemmich and Gilson, 2009) (https://sio-argo.ucsd.edu/RG_Climatology.html, accessed on 23 July 2021). The RG has 27 vertical levels and $1^\circ \times 1^\circ$ spatial resolution from the surface to 2000 m. To estimate the mean-field, RG Argo Climatology uses weighted least-squares fitting the nearest 100 Argo profiles within a certain month. The RG Argo climatology periods used in this study are from January 2004 to December 2020.

The other dataset for comparison to RG is monthly gridded of salinity and temperature from the Grid Point Value of the Monthly Objective Analysis using the Argo data (MOAA-GPV) (Hosoda et al., 2008) from Japan Agency for Marine-Earth Science and Technology (JAMSTEC) in 2004–2015 (http://www.jamstec.go.jp/, accessed on 1 July 2018). The MOAA-GPV has 25 vertical levels and $1^\circ \times 1^\circ$ spatial resolution from the surface to 2000 m.

2.1.2. Atmospheric variables

Monthly averaged evaporation (E) and precipitation (P) are utilized to investigate the sea surface freshwater flux from the atmosphere. Monthly averaged zonal and meridional wind velocity are also used to examine the wind stress over the Indo-Pacific region. The atmospheric variables product used in this study is the reanalysis data from European Centre for Medium-Range Weather Forecasts (ECMWF) Reanalysis v5 (ERA5) (Hersbach et al., 2020). The ERA5 covers the Earth on a 30km grid from 1950 to the present. ERA5 is produced by the Copernicus Climate Change Service (C3S) at ECMWF (https://cds.climate.copernicus.eu/cdsapp#!/dataset/reanalysis-era5-single-levels-monthly-means?tab=form, accessed on 23 July 2021).

The monthly mean of evaporation (E) and precipitation (P) from the Japanese 55-year reanalysis (JRA55) are used for comparison with the ERA5 dataset. This is used to determine the robustness of changes in freshwater fluxes. The JRA55 has a horizontal resolution of $1.25^\circ \times 1.25^\circ$ (https://rda.ucar.edu/datasets/ds628.0/, accessed on 1 Ma y 2022).

2.1.3. ITF

The ITF transport is estimated along the section at 114°E in the Indian Ocean (114°E and 8.3°–22°S) based on the 3-hourly Hybrid Coordinate Ocean Model - Global Ocean Forecasting System (HYCOM-GOFS 3.1) with 1/12° horizontal resolution. A previous study by Metzger et al. (2010), found that HYCOM represents well with the observation of ITF transport in various straits in the Indonesian Seas, primarily distributed correctly among the three outflow passages (Lombok Strait, Ombai Strait, and Timor Passage) (http://www.hycom.org/, accessed on 16 May 2022).

2.1.4. Sea level anomalies

The monthly averaged sea level anomaly (SLA) used in this study is from Aviso products (0.25° resolution). SLA is derived from Ssalto/Duacs multimission altimeter from January 1993 to the last extension of the delayed-time products. The long delayed-time dataset is used to compute statistical means of mean SLA over different periods. Averaged mean SLA and Climatological mean SLA is created from daily Ssalto/Duacs – Delayed-time mean SLA (DT MSLA) - Merged Product (ftp://ftp-access.aviso.altimetry.fr/climatology, accessed on 23 July 2021).

2.1.5. Niño 3.4 index and Dipole Mode Index (DMI)

El Niño events in this study are detected by the Niño 3.4 index from World Meteorological Organization (https://climexp.knmi.nl/getindices.cgi, accessed on 23 July 2021). Nino 3.4 index is derived from SST Optimum Interpolation version 2 (OI.v2) anomalies in the Niño 3.4 region at 120°–170°W, and 5°N–5°S.

Dipole Mode Index (DMI) is used to determine the Indian Ocean Dipole (IOD) events. DMI is represented by the SST anomalies gradient between the western equatorial Indian Ocean (50°E-70°E and 10°S-10°N) and the southeastern equatorial Indian Ocean (90°E-110°E and 10°S-0°N). DMI is based on daily Reynolds OI. v2 SST analysis accessed from the National Oceanic and Atmospheric Administration (NOAA) (https://stateoftheocean.osmc.noaa.gov/sur/ind/dmi.php, accessed on 23 July 2021).

2.2. Methods

The area of study is 30°–180° E and 30°N–30°S, which covers the full of the Indian Ocean and western tropical Pacific Ocean. Specifically, to observe the change of water masses in a certain location across the Maritime Continent during the RG period (beginning in January 2004), the water masses in the outflow of ITF are observed (number of profiles of Argo floats in box region can be seen in the supplementary material in Figure S1). In Figure 1c, the outflow of ITF is defined at 93.5°–125.5°E

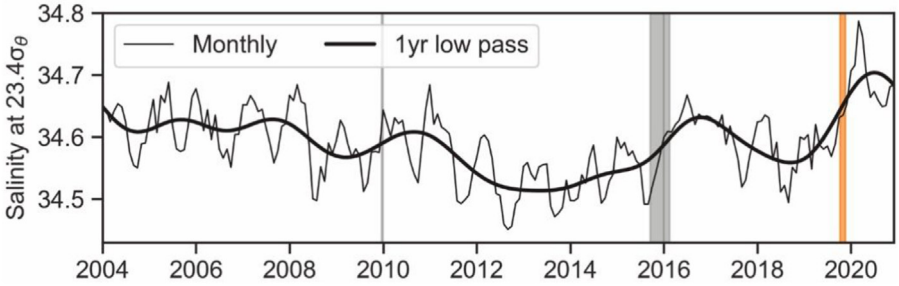

Figure 2. Time series of monthly mean salinity at IUW density range (σ_θ = 22.00–26.00 kg m^{-3}) in the outflow of ITF. Thick lines represent 1-year Butterworth low-pass filter. Grey and orange shade bar indicate strong El Niño and IOD events, respectively. Strong event is defined when the daily index >2.0.

and 7.5°–16.5°S. Maritime Continent in this paper is referenced primarily by the region enclosed by 95.5°E–140.5°E and 9.5°N–15.5°S (Figure 1c). The Maritime Continent box covers all the land and marginal seas in the Indonesian area. The outflow of the ITF region in the Indian Ocean is selected for tracing temperature and salinity signals in our depth–time analysis. The outflow box in the Indian Ocean captures the Indonesian Upper Water characteristics as it is close to its source region in the Indonesian Seas before its characteristics disappear due to interaction with saltier water from the Indian Ocean (Talley and Sprintall, 2005). The IUW in this study is characterized by a temperature of 11.00–23.00 °C and salinity of 34.40–35.00 psu that lies at the density of σ_θ = 22.00–26.00 kg m^{-3}. Below this density, there are fresher IIW (T = 3.50–5.50 °C; S = 34.60–34.70 psu; σ_θ = 27.00–27.50 kg m^{-3}) (Talley and Sprintall, 2005) and distinct high salinity water masses from the Indian Ocean (Figure 1b).

The potential density anomaly relative to surface depth (σ_θ) is derived from the monthly temperature and salinity fields (TS) of the RG product. Potential density anomaly is calculated by the Gibbs Sea Water of TEOS-10 (McDougall and Barker, 2011). As water masses move along the isopycnal surface, the temperature-salinity (T-S) is estimated based on the potential density coordinate.

The ERA5 global atmospheric reanalysis product (Hersbach et al., 2020) determines atmospheric freshwater flux by evaporation minus precipitation (E-P). ERA5 products also provide wind velocity fields that can be used to calculate wind stress curl. Vector wind stress fields are determined by $\tau = \rho_{air} C D u^2$, where τ is the vector wind stress field in the zonal (τ_x) or the meridional (τ_y) direction, u is vector wind velocity (zonal or meridional), CD is drag coefficient (Yelland and Taylor, 1996), and ρ_{air} is density of air at 1.225 kg m^{-3}.

Changes in salinity, freshwater flux (E-P), wind, and sea level anomalies are performed for each data grid and estimated by linear trends. The seasonality of particular products is removed before calculating the trend/change by using Butterworth low pass filter. The Mann-Kendall statistical test is applied in the trend detection of the time series.

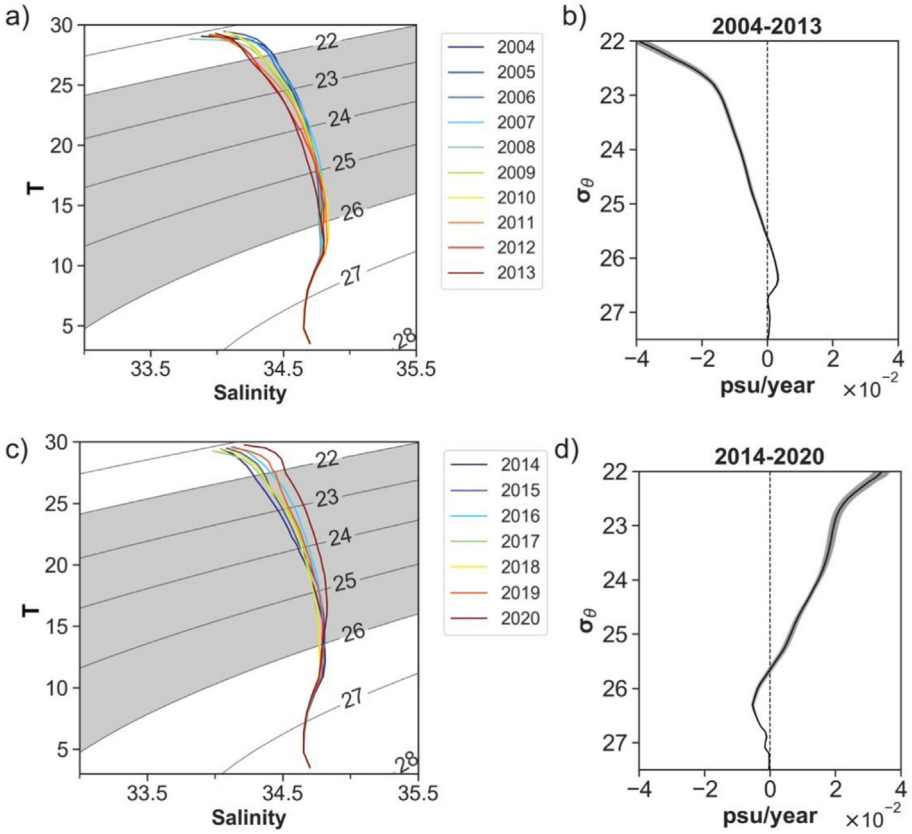

Figure 3. (a) Annual mean TS diagram for outflows of ITF, 2004–2013, and (b) its salinity changes (psu year^{-1}) along isopycnal surface; (c) and (d) are similar to (a) and (b) except for 2014–2020. The black thick line represents the average, and the light shadings represents two standard error. The gray shaded contours in Figures (a) and (c) represent the IUW density range (σ_θ = 22.00–26.00 kg m^{-3}) used in this study.

Mann-Kendall test trend is used to analyze the consistently increasing or decreasing (monotonic) trends over time periods (Yue and Wang, 2004).

The cross-correlation coefficient analysis is performed to find the lag between the two time series, the methodology followed by Emery and Thomson (2001). The analysis is performed in several cases, i.e., (1) E-P in Maritime Continent and IUW salinity (density range $\sigma_\theta = 22.00–26.00$ kg m^{-3}) in the outflow of ITF to understand the correlation between freshwater flux in Maritime Continent and salinity in the Indian Ocean at IUW depth level, (2) ITF transport and IUW salinity in the outflow of ITF, (3) Nino3.4 index and E-P in Maritime Continent to find the correlation between ENSO and freshwater flux in Maritime Continent, and (4) DMI and E-P in Maritime Continent to find the correlation between IOD and freshwater flux in Maritime Continent.

3. Results and Discussion

3.1. Changes in the salinity of the IUW in the outflow of the ITF

The time series of mean salinity in the IUW density range (σ_θ = 22.00–26.00 kg m^{-3}) is presented in Figure 2. Figure 2 shows that IUW salinity in the ITF outflow decreases from 2004 to 2013 and increases from 2014 to the remaining periods. Nonetheless, salinity from 2016-2017 is increased abruptly, followed by a slight reduction in 2019, until it reached the highest salinity in late 2019 to 2020. The water masses from late 2019 to 2020 are particularly saline compared to the other periods. The regional salinity anomalies in the outflow of ITF could be affected by one of the strongest recorded El Niño in 2015–2016.

On the vertical structure, the water masses in the outflow of ITF consist of the IUW from the surface to the thermocline depth and underlying IIW (Talley and Sprintall, 2005). The annual mean of the TS diagram in the ITF outflow is shown in Figure 3, which shows a shift in the TS diagram over the 2004–2020 period. As shown in Figure 3a, during the 2004–2013 periods, the shift to low salinity and low temperature in the TS diagram can be observed up to a density of $\sigma_\theta = 25.5$ kg m^{-3} where the IUW exists, indicating freshening in the water column. The change in salinity, as shown in Figure 3b, implies that freshening occupies most of the IUW layer during 2004–2013, except for the layer at $\sigma_\theta = 25.5$ kg m^{-3}, which is slightly saline in the intermediate layer. In contrast, as shown in Figures 3c and 3d, during 2014–2020, the shift to high salinity and high temperature can be observed in the TS diagram that reflects the reversal condition from the 2004–2013 periods. We find that there are no notable changes in salinity in the entire period from 2004 to 2020. Specifically, there is no significant change in salinity in the outflow of the ITF, which shows the trend or changes in salinity that are close to zero (supplementary material, Figure S2). This can also be observed far into the Indian Ocean at the thermocline. Therefore, in this study, the explanation for the following part is divided into two periods.

In addition to the IIW, there is another distinct water mass in the central part of the Indian Ocean in the layer below $\sigma_\theta = 25.5$ kg m^{-3}, which is characterized by extremely high salinity and originates from the Indian Ocean (see Figure 1b). Talley and Sprintall (2005) suggest that this extremely high salinity in the central Indian Ocean, which extends into the southeastern Indian Ocean, is originated from Arabian surface waters and Indian deep waters. In Figures 3b and 3d, the water below $\sigma_\theta = 25.5$ kg m^{-3} (where the high salinity from the Indian Ocean and IIW is present) experiences salinification, which is shown as a positive change during 2004–2013 and freshening during 2014–2020. It is noted that these changes in high salinity Indian Ocean waters could also be induced by the changes of evaporation and precipitation in the formation area along with other processes. However, further investigation is beyond the scope of this study.

Re-plots of Figure 3 using another Argo gridded product from JAMSTEC MOAA-GPV are also shown for comparison in the periods 2004–2013 to reveal the robustness of salinity variations displayed by the RG data (see Figure S3 in the supplementary material, note that due to data availability, the result is only done for 2004–2013). A similar change in salinity along the density surfaces in the thermocline and intermediate layers is also observed in the outflow of the ITF in the MOAA-GPV dataset. The main discrepancy between RG and MOAA-GPV is the rate of salinity change in RG, which is lower than in MOAA-GPV at a 95% confidence level. Nevertheless, it clearly shows that there is salinification in the IIW core at $\sigma_\theta = 27.3$ kg m^{-3}, which is presented as a positive

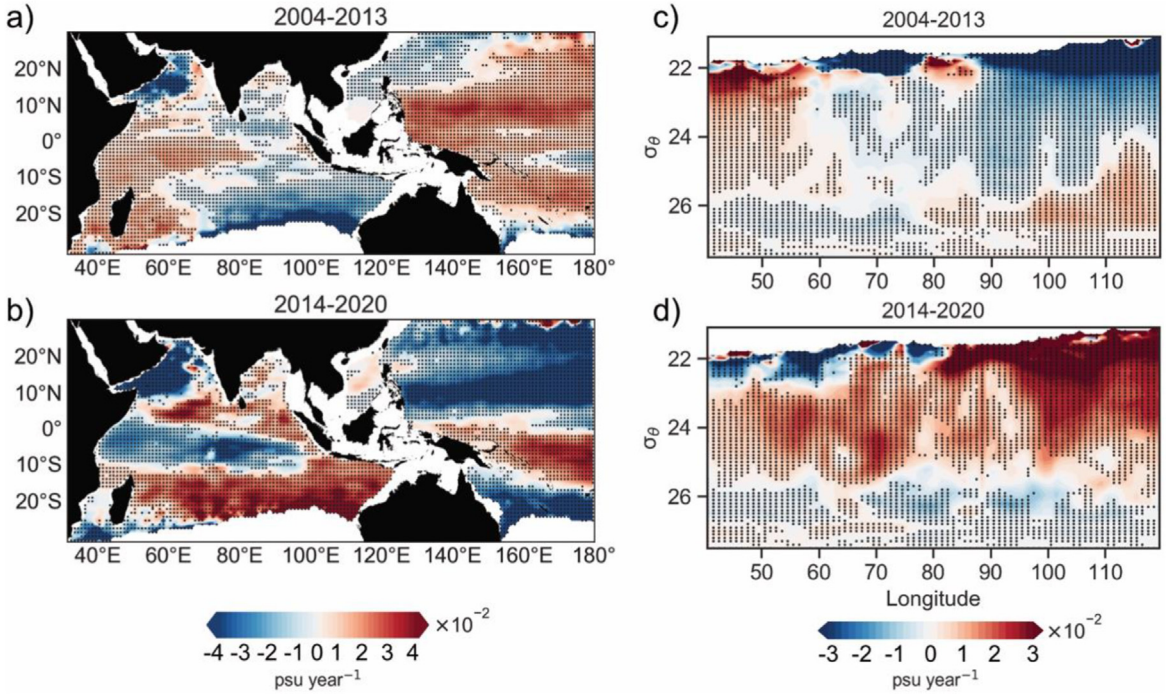

Figure 4. The change in salinity at $\sigma_\theta = 23.4$ kg m^{-3} (psu year^{-1}) in the western tropical Pacific Ocean and the Indian Ocean during (a) 2004–2013 and (b) 2014–2020. The change in salinity (psu year^{-1}) along 12.5°S in the Indian Ocean on σ_θ coordinate during (c) 2004–2013 and d) 2014–2020. At 95% confidence levels, the dots represent regions with a significant linear trend based on the Mann-Kendall test.

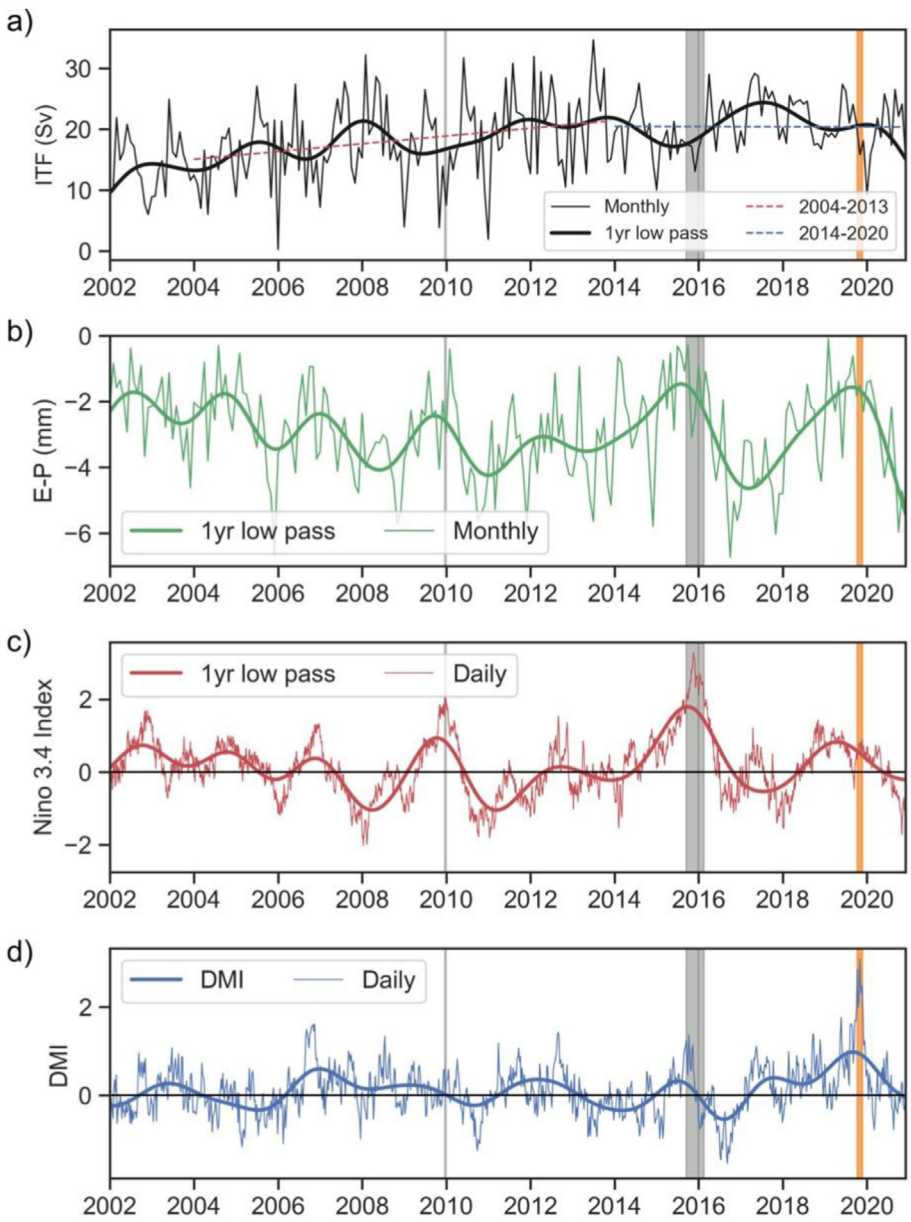

Figure 5. (a) Time series of monthly mean ITF transport (Sv), (b) monthly mean of E-P (mm day $^{-1}$) in Maritime Continent (grey box in Figure 1c at 95.5°E-140.5°E and 9.5°N-15.5°S), (c) Nino 3.4 index and (d) Dipole mode index (DMI) from January 2002 to December 2020. Thick lines represent 1-year Butterworth low-pass filter. Grey and orange shade bar indicate strong El Niño and IOD events, respectively. Strong event is defined when the daily index >2.0. The dashed line in Figure (a) represents the regression line from 2004-2013 (red) and 2014–2020 (blue).

change. The overall changes and consistency of salinity changes over the 2004–2013 period indicated by the RG and MOAA GPV data suggest that the freshening of the IUW is robust.

In short, there are fairly opposite salinity distributions in the outflow of ITF, with the negative (positive) change in salinity is observed during the period of 2004–2013 (2014–2020). To see the salinity changes over the large-spatial scale, therefore, we provide the changes in water masses at one isopycnal surface of $\sigma_\theta = 23.4$ kg m^{-3} in the thermocline. Analysis of salinity at $\sigma_\theta = 23.4$ kg m^{-3} is performed by examining a subset of RG products in a monthly field between 2004 and 2020. The spatial map of a linear change in salinity is calculated in two time periods, as done previously, from 2004 to 2013, and 2014–2020. We show the spatial map of the linear change in salinity in the Indo-Pacific region at $\sigma_\theta = 23.4$ kg m^{-3} in Figure 4, which is obtained in annual units (psu/year) for each grid point. As shown in Figure 4a, according to this subset of RG products, the salinity has decreased in large parts of the southeastern Indian Ocean. In particular, negative changes are observed farther east of the Indian Ocean, suggesting that the freshening of IUW is robust. The MOAA-GPV datasets also indicate that a significant decrease in salinity occurs in the thermoclines of the southeastern tropical Indian Ocean compared to the southwestern tropical Indian Ocean (see supplementary material Figure S3). As shown in Figure 4b, an opposite change in salinity is observed during the 2014–2020 period, with the positive change occurring in most regions of the southeast Indian Ocean, suggesting salinification of the IUW during this period. In addition, as shown in Figure 4c, from 2004-2013, another notable difference is that the negative change in the eastern Indian Ocean is also observed at much greater depths than on the western side. A vertical section of the linear trend/change indicates that the decrease in salinity is occupied at the top of $\sigma_\theta = 25.5$ kg m^{-3} on the east side. This decrease-salinity signal attenuates on the west side, where the positive change is most common. The negative change is observed deeper than $\sigma_\theta = 25.5$ kg m^{-3} (intermediate layer), farther east in the center of the Indian Ocean. In Figure 4d, the reverse change in the distinct regional salinity is also evident in the

vertical section, where the increase in salinity is observed in the upper σ_θ = 25.0 kg m^{-3} and is concentrated on the eastern side of the Indian Ocean, while a decrease in salinity is observed below σ_θ = 25.5 kg m^{-3}.

3.2. Oceanic and atmospheric conditions in the maritime continent

This section focuses on the ocean-atmospheric condition related to the salinity decline or incline of the thermocline IUW in the Indian Ocean. The decrease or increase in salinity in the IUW layer suggests that such a change could be triggered by freshwater input from the source region in the Maritime Continent. Although the mixing with local freshwater input also gives rise to a salt loss from the surface layer, in this study, we concentrate on analyzing salinity change in the thermocline with its relationship from several parameters in the Maritime Continent on the large-spatial scale perspective.

Time series of ITF, freshwater flux (E-P) in Maritime Continent, Nino 3.4 index, and DMI are presented in Figure 5. Figure 5a shows the total ITF transport (ITF) estimated along 114°E from HYCOM. From 2004 to 2013, ITF experienced a significant increase (1.74×10^{-3} Sv month^{-1}), while from 2014 to 2020, the ITF decreased slightly with a relatively constant tendency (-4.42×10^{-5} Sv month^{-1}). This result shows that the decreasing salinity in the thermocline during 2004–2013 is accompanied by an increase the ITF transport. Figure 5a also shows that the minimum ITF transport is accompanied by the strong El Niño event in 2015/2016. The previous studies also reported that the ITF transport is weaker during El Niño and stronger during La-Niña due to the influences of the large-scale tropical ocean-atmosphere interaction and Pacific waveguide (England and Huang, 2005; Feng et al., 2018).

The atmospheric freshwater flux plays a vital role in determining the spatial pattern of salinity in oceans, which is determined by the difference between evaporation and precipitation. The decrease in maximum salinity in 2013 in Figure 2 suggests that there is freshwater input from freshwater fluxes in the Maritime Continent that is carried to the ITF outflow. As shown in Figure 5b, E-P on the Maritime Continent decreased between 2002 and 2010, reflecting increasing freshwater input from the atmosphere, and it increased again in 2011. The low freshwater flux in 2015–2016 indicates evaporation dominated the period. In Figure 5c, this low freshwater flux is associated with the strong El Niño event in 2015. El Niño persisted in 2015 and subsided in austral autumn of 2016 (Benthuysen et al., 2018). Figure 5c also shows that there was a short time and fairly strong El Niño in 2009–2010. El Niño years are associated with shifts in Walker circulation and later onset-weaker Australian summer monsoons (Benthuysen et al., 2018; Redondo-Rodriguez et al., 2012). El Niño is related to high outgoing longwave radiation and cloud cover reduction across low-latitude Australasia (Allan and Pariwono, 1990; Klein et al., 1999). As the strong El Niño decayed at the end of 2016, the Dipole Mode Index (DMI) became negative, as shown in Figure 5d, which appears as one of the strongest negative indices at the end of 2016, signifying relatively high freshwater flux lasted through 2017 in the Maritime Continent. It is worth noting that the Nino 3.4 index is negative during this period. The high salinity in late 2019 to 2020 could be influenced by the strongest positive IOD during these periods. It also shows that the freshwater flux on the Maritime Continent is low along with the peak of the DMI.

The long-term mean E-P in the tropics is negative because precipitation exceeds evaporation over time. However, the acceleration of the global hydrologic cycle could impact the E-P (Durack et al., 2012), leading to more precipitation relative to evaporation in the equatorial region, including the Maritime Continent. Figure 5b shows that the E-P in the Maritime Continent tends to fluctuate in a certain period. The periods of the E-P decline remarkably occurred from 2002-2010. Then it started to incline in the following years until it reached the maximum at the end of 2019, after which E-P declined until the end of 2020. Nonetheless, there was a substantial decline in E-P in 2017 associated with the strongly negative IOD events. The decreasing trends/change of E-P in the Maritime Continent during 2002–2010 in Figure 5b as much -5.19 × 10^{-4} mm day^{-1} month^{-1} from ERA5 reanalysis dataset and the increasing trend/change as much 7.50 × 10^{-5} mm day^{-1} month^{-1} during 2011–2018.

In Figure 6, lead-lag correlation analysis is presented as the lag (in months) between the peak of two-time series events. Positive lags represent delays, and negative lags represent leads between two-time series. The cross-correlation between salinity at the IUW layer (σ_θ = 22.00–26.00 kg m^{-3}) and freshwater flux (red line) shows that freshening-salinification in the outflow of ITF is correlated with the pattern of freshwater flux in the Maritime Continent. However, in this relationship, salinity is delayed by 13 months. This suggests that the change of freshwater input in the Maritime Continent could be one possible mechanism that induces the fluctuation of salinity in the outflow of ITF. A previous study by Hu and Sprintall (2017) also shows that freshwater input to the Maritime Continent led to enhanced ITF, and its freshwater transport is responsible for freshening in the eastern Indian Ocean. Interestingly, El Niño and freshwater flux in the Maritime Continent have a strong correlation (0.8) that shows a positive correlation at zero-time lag, as shown in Figure 6 (blue line). Therefore, it implies that El Niño could play a key role in regulating atmospheric freshwater flux in the Maritime Continent. While DMI and freshwater flux in the Maritime Continent (green line) show a low correlation (0.3). The ITF is negatively correlated with IUW salinity in the ITF outflow with 12 month time lag, indicating that the stronger the ITF, the fresher the salinity in the Indian Ocean, and vice versa (black line). It is worth noting that the enhanced effect of ITF on the decreasing salinity occurred during 2004–2013. Hu et al. (2019) show that the El Niño-Southern Oscillation (ENSO) and Pacific Decadal Oscillation (PDO) modulate salinity variations in the southeastern Indian Ocean and predict a 10-month lead time between Indian Ocean salinity and the PDO index. They also show that the ITF plays an important role in transferring ENSO- and PDO-related signals to the Indian Ocean.

When the linear spatial change of E-P in the Indo-Pacific region is divided into two different time periods (2002–2010 and 2011–2018), notable differences appear with respect to the changes that are observed in the Maritime Continent compared to the southeastern Indian Ocean and western tropical Pacific Ocean. The spatial map of the E-P trends/change of those two time periods can be seen in Figure 7. The 2002–2010 and 2011–2018 period is selected because the time lag between E-P and salinity occurs around ~1–2 years, and the most obvious pattern represented as a decrease-increase in E-P (increase-decrease freshwater flux) is present in the time series that correspond the tendency of salinity. In Figure 7a, there is a decreasing imbalance between precipitation and evaporation in the Maritime Continent from 2002 to 2010. The change in E-P is mostly negative in almost all of the Maritime Continent box, which indicates the dominant precipitation. As shown in Figure 7a, an increased air-sea freshwater flux is also observed in the South Pacific Convergence

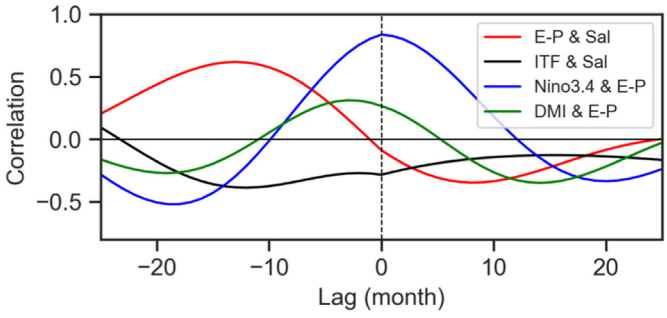

Figure 6. Correlation analysis at monthly lag intervals between E-P in Maritime Continent and IUW salinity (= 22.00–26.00 kg m^{-3}) in the outflow of ITF (red), ITF and IUW salinity in the outflow of ITF (black), Nino3.4 index and E-P in Maritime Continent (blue), and DMI and E-P in Maritime Continent (green). Positive lags represent delays, and negative lags represent leads between two-time series.

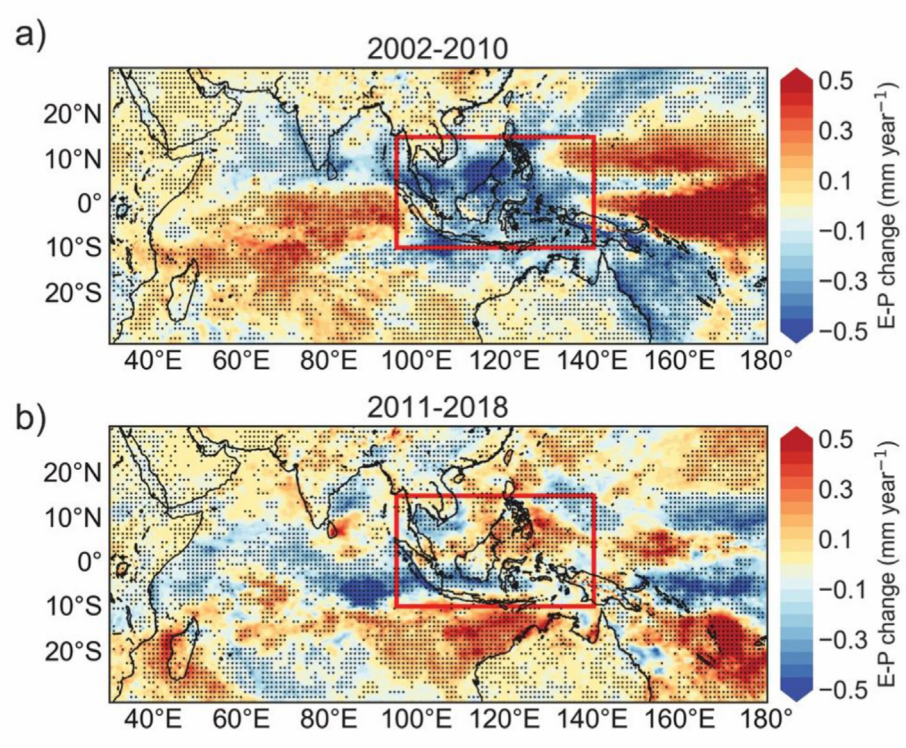

Figure 7. The change in E-P (mm year^{-1}) in the western tropical Pacific Ocean, Maritime Continent, and the Indian Ocean from (a) 2002–2010, and (b) 2011–2018. At 95% confidence levels, the dots represent regions with a significant linear trend based on the Mann-Kendall test. The red box region indicates the Maritime Continent.

Zone (SPCZ) near New Guinea Island, extending to northeastern tropical Australia, where changes in salinity at the thermocline are not negative compared to the southeastern Indian Ocean. The positive change of E-P is observed in the equatorial Pacific Ocean extending from 10°N to 10°S, and in the middle of the Indian Ocean, where the change is much smaller than in the equatorial Pacific Ocean. In contrast to the change during

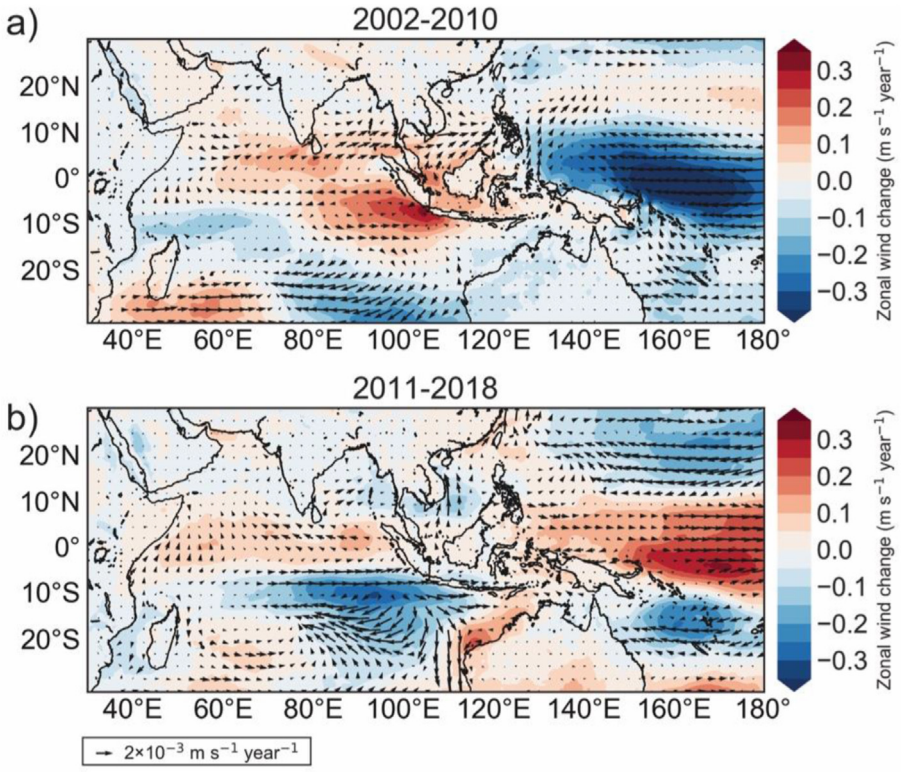

Figure 8. The change in wind stress (N m^{-2} year^{-1} in vector), and zonal wind (m s^{-1} year^{-1} in shade color) in the western tropical Pacific Ocean, Maritime Continent, and the Indian Ocean from (a) 2002–2010, and (b) 2011–2018.

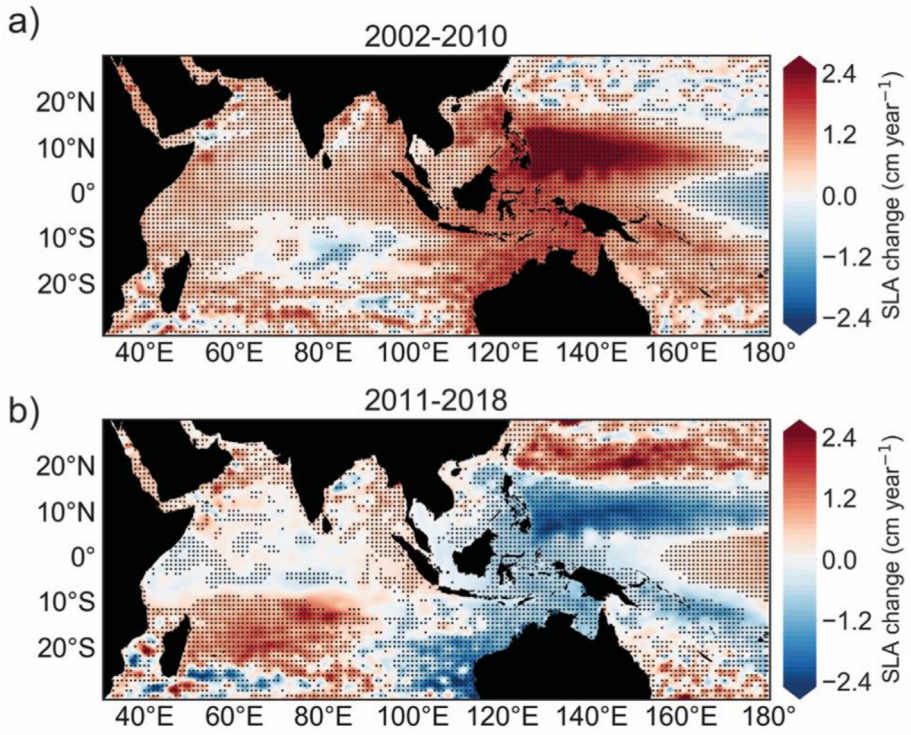

Figure 9. The change in sea sea-level anomalies (cm year^{-1}) from Aviso in the western tropical Pacific Ocean, Maritime Continent, and Indian Ocean from (a) 2002–2010, and (b) 2011–2018. At 95% confidence levels, the dots represent regions with a significant linear trend based on the Mann-Kendall test.

2002–2010, the examination of E-P change in the Maritime Continent from 2011-2018 is generally positive (Figure 7b). It appears that the increasing imbalance between precipitation and evaporation is not only found in the Maritime Continent but also in northwestern tropical Australia and a small part of SPCZ. The positive change in E-P indicates that evaporation takes place in regulating the freshwater flux. The regions where the positive change is found in the equatorial Pacific Ocean during 2002–2010 are reversed, which shows a negative change during 2011–2018. Re-plots of Figure 7 using JRA55 are also shown for comparison to ERA5 (see Figure S5 in the supplementary material). An opposite change in freshwater flux between the 2002–2010 and 2011–2018 periods is also detected in the JRA55. It clearly shows that most of the regions in the Maritime Continent have a negative change during 2002–2010, and it is reversed in the following periods. The overall changes and consistency of freshwater flux changes over the entire period are robustly represented by the ERA5 and JRA55 data. Figure 8 shows the wind stress (vector) and zonal wind change in the two time periods (2002–2010 and 2011–2014) from the reanalysis of ERA5 products. During 2002–2010, in Figure 8a, we observe significant zonal wind changes in the southeastern Indian Ocean and western tropical Pacific Ocean. The change in zonal winds in the western tropical Pacific is weak and westward, which opposes the mean westerly wind direction. In the southeastern Indian Ocean, a marked increase in zonal wind is observed. The change of wind stress (vector) displays a strong zonal wind-stress in the eastward direction over the southeastern Indian Ocean compared to the other regions. This result implies during this period, the wind both in the equatorial Pacific Ocean and the Indian Ocean tends toward the Maritime Continent.

The opposite zonal wind and wind stress linear trend/change pattern during 2011–2018 are shown in Figure 8b, with strong zonal wind directed eastward in the western Pacific Ocean and weak zonal wind directed westward in the southeastern Indian Ocean. Generally, the wind pattern tends to shifts away from the Maritime Continent. The dominance of the positive zonal wind trends/changes in the western Pacific Ocean is remarkable compared to the positive change over the regions. Our investigation points to the predominance of accelerating or decelerating winds tendency that corresponds to freshwater flux patterns in the Maritime Continent in general, leading to strengthening wind towards Maritime Continent with greater freshwater flux and weakening wind towards Maritime Continent with lower freshwater flux.

In addition to wind changes, in Figure 9, we also determine a sea-level anomaly change over two time periods. As shown in Figure 9a, changes in sea level anomaly (SLA) from altimetry show a significant upward change in Maritime Continent and the northern Indian Ocean, with the most prominent in the western tropical Pacific during 2002–2010. It is worth noting that the SLA changes in the western Pacific Ocean is more positive than the outflow of ITF in the southeastern Indian Ocean, and the negative changes are found in the central Pacific and Indian Oceans. In contrast, as shown in Figure 9b, these trends/changes are reversing, with a decreasing change is observed in the Maritime Continent and an increasing changes in the central Pacific and Indian Oceans during 2011–2018.

This rise and fall of sea level further reflect the strength and shape of the wind-driven in the Indo-Pacific region, which is considered to be a qualitative measure of the atmospheric circulation. Anomalously higher (lower) sea levels change in the western tropical Pacific coincides with weaker (stronger) zonal wind implying the tendency of the wind directed eastward to (westward from) Maritime Continent. The previous studies also found that the increase in precipitation coincides with the shift of winds (Du et al., 2015; Hu and Sprintall, 2016). Their results show that the far west of the Pacific experiences stronger easterly winds. In the Indian Ocean, the westerly wind weakens and therefore coincides with the strengthening of precipitation over the Maritime Continent. This rise and fall of sea level in the western tropical Pacific (as well as in the southeastern Indian Ocean) is essential because it regulates the ITF (Feng et al., 2018; Gordon, 2005; Wyrtki, 1961), which means that ITF

transport is high when there is a notable difference in the pressure gradient between the western tropical Pacific and the southeastern Indian Ocean.

4. Conclusions

Recent changes in the mean salinity of the IUW in the southeastern Indian Ocean are investigated from Argo products. A subset of salinity changes shows a unique tendency representing the opposite salinity changes over two time periods. There are large data gaps in Argo products inside Indonesian seas, which mostly related to regions where Argo floats coverage is inadequate or largely absent. Thus, the salinity changes of IUW could not be estimated from its formation region in the Indonesian Seas, but it is established by observing salinity changes of IUW in the outflow of ITF. From 2004 to 2013, RG gridded data indicate a basin-scale freshening of the IUW in the Indian Ocean. The opposite changes appear for the period from 2014 to 2020, where IUW shows a general increase in salinity, especially in the southeastern Indian Ocean.

Multiple processes could influence salinity changes in the Indo-Pacific region, and the dominant process varies on the annual basis. While increases (decreases) in freshwater fluxes are likely to have contributed to widespread freshening (salinification) of the IUW, leading to the alleged of low-salinity (high-salinity) waters from the source region of IUW in the Indonesian Seas.

This change in salinity is also enhanced by changes in ITF, especially during the period 2004–2013. The enhanced ITF represents the accelerated transport of water masses from the Indonesian seas to the Indian Ocean. In the next period, evaporation will be more dominant in the Indonesian seas, indicating that salinity in the Indonesian seas tends to be high, and the ITF transports this high salinity water to the Indian Ocean. Therefore, an increase or decrease in freshwater flux and ITF are suggested to be a crucial factor in determining salinity changes in the southeastern Indian Ocean. Changes in freshwater flux in the Maritime Continent are directly correlated with the El Niño, with an associated zero-time lag. Nonetheless, a decline in freshwater flux in 2019 seems to be associated with strong positive IOD (time lag of 3 months). However, the cause of which is out of the scope of this study.

Generally speaking, the changes in precipitation over the Maritime Continent induce a salinity change of the IUW in the southeastern Indian Ocean. The freshwater forcing in the Maritime Continent could determine the basin-scale patterns of surface salinity, whereas the ocean dynamic processes would restructure its distribution so that it is transferred to the thermocline. Horizontal advection of ocean currents in relation to ocean transport could affect the strength and spatial distribution of the thermocline salinity change in the southeastern Indian Ocean. These results have been shown in this study by explaining two different cases in the Argo periods, in which the decline and incline salinity in the southeastern Indian Ocean. Similar to previous studies, such as Du et al. (2015), this study suggests that a large part of freshwater flux in the Maritime Continent is associated with Walker Circulation and plays a major role in determining the observed salinity changes in the southeastern Indian Ocean. The fluctuation of salinity changes in the Indo-Pacific region is explained by the fluctuation, in association, of the ocean-atmospheric forcing.

Even though the salinity tendency such as influence of local freshwater flux, entrainment and vertical mixing, as well as the influence of the inflow intermediate water to the IUW are not examined in this study, by a qualitative analysis, the results in this study imply that during residence in the Indonesian Seas, the inflow Pacific water is modified by the input of atmospheric freshwater flux in the Maritime Continent, so that the IUW in the formation region in Indonesian Seas experiences basin-scale salinity changes, and is transferred to the Indian Ocean by the ITF.

Hu and Sprintall (2017) found that increased precipitation over the Maritime Continent freshens the Indonesian seas and enhances the volume transfer of the ITF, which is attributed to a freshening and subsequent increase in the halosteric component of the ITF transport. They also argue that local precipitation in Indonesian seas is an important source of salinity anomaly signals in the ITF movement. Our study agrees with a previous study (Hu and Sprintall, 2016, 2017), which mentions that the intensification of ITF transport causes a significant change in freshwater exchanges between the Pacific and Indian Oceans, leading to the freshening of the eastern Indian Ocean. In short, the increased rainfall in the Indonesian seas results in a large freshwater input to the Indian Ocean, which is accelerated by the ITF. This can be seen in the two contrasting phenomena of salinity in the Indian Ocean between 2004-2013 and 2014–2020, which are related to changes in freshwater input in the Indonesian Seas during the two periods. The zonal shift in the Walker circulation coincides with a change in precipitation over the Indonesian Seas, which is the main source of freshwater input and is possibly controlled by the ENSO cycle. It is suggested that the incoming Pacific water, which becomes saline in the thermocline, is vigorously mixed with local freshwater input by tidal mixing as it enters the Indonesian Seas.

This work is intended to disclose the IUW salinity change in the outflow of ITF over the last 16-year period; in particular, the mechanisms contributing to the freshening and salinification signal in the IUW in the large-scale perspective are also described. For a detailed explanation of the changes in salinity, the other factors must be examined comprehensively, i.e., surface mixing should be known as well as IUW variability in the formation region. The quantification of these contributors and their influence on global hydrodynamic patterns should be the focus of future research.

Declarations

Author contribution statement

Mochamad Riza Iskandar: Conceived and designed the experiments; Performed the experiments; Analyzed and interpreted the data; Wrote the paper.

Toshio Suga: Conceived and designed the experiments; Analyzed and interpreted the data; Wrote the paper.

Funding statement

Toshio Suga was supported by JST SICORP [JPMJSC21E7].

Data availability statement

Data associated with this study has been deposited at the Roemmich-Gilson Argo Climatology (https://sio-argo.ucsd.edu/RG_Climatology.html).

Declaration of interests statement

The authors declare no conflict of interest.

Additional information

Supplementary content related to this article has been published online at https://doi.org/10.1016/j.heliyon.2022.e10430.

Acknowledgements

Special thanks to Prof. Kimio Hanawa from Tohoku University (currently in Yamagata University) for the meaningful discussion. We also thank reviewers for improving the quality of the paper. M.R.I. is the main author of this manuscript, a substantial part of this work was conducted at Tohoku University as a scholarship student supported by the Ministry of Education, Culture, Sports, Science, and Technology (MEXT) of the Japanese government and the International Joint Graduate Program in Earth and Environmental Sciences (GP-EES) of Tohoku University.

References

Allan, R.J., Pariwono, J.I., 1990. Ocean-atmosphere interactions in low-latitude Australasia. Int. J. Climatol. 10, 145–178.

Benthuysen, J.A., Oliver, E.C.J., Feng, M., Marshall, A.G., 2018. Extreme marine warming across tropical Australia during austral summer 2015–2016. J. Geophys. Res. Ocean. 123, 1301–1326.

Boyer, T.P., Levitus, S., Antonov, J.I., Locarnini, R.A., Garcia, H.E., 2005. Linear trends in salinity for the world ocean, 1955-1998. Geophys. Res. Lett. 32.

Chou, C., Neelin, J.D., Chen, C.-A., Tu, J.-Y., 2009. Evaluating the "rich-get-richer" mechanism in tropical precipitation change under global warming. J. Clim. 22, 1982–2005.

Cravatte, S., Delcroix, T., Zhang, D., McPhaden, M., Leloup, J., 2009. Observed freshening and warming of the western pacific warm pool. Clim. Dynam. 33, 565–589.

Dong, B., Dai, A., 2015. The influence of the interdecadal pacific oscillation on temperature and precipitation over the globe. Clim. Dynam. 45, 2667–2681.

Du, Y., Zhang, Y., Feng, M., Wang, T., Zhang, N., Wijffels, S., 2015. Decadal trends of the upper ocean salinity in the tropical Indo-Pacific since mid-1990s. Sci. Rep. 5, 16050.

Durack, P.J., Wijffels, S.E., Matear, R.J., 2012. Ocean salinities reveal strong global water cycle intensification during 1950 to 2000. Science 336 (80-), 455–458.

Emery, W.J., Thomson, R.E., 2001. Chapter 2 - data processing and presentation. In: Emery, W.J., Thomson, R.E. (Eds.), Data Analysis Methods in Physical Oceanography. Elsevier Science, Amsterdam, pp. 159–191.

England, M.H., Huang, F., 2005. On the interannual variability of the Indonesian throughflow and its linkage with ENSO. J. Clim. 18, 1435–1444.

Feng, M., Zhang, N., Liu, Q., Wijffels, S., 2018. The Indonesian throughflow, its variability and centennial change. Geosci. Lett. 5.

Ffield, A., Gordon, A.L., 1996. Tidal mixing signatures in the Indonesian seas. J. Phys. Oceanogr. 26, 1924–1937.

Fieux, M., Andrié, C., Delecluse, P., Ilahude, A.G., Kartavtseff, A., Mantisi, F., Molcard, R., Swallow, J.C., 1994. Measurements within the pacific-Indian oceans throughflow region. Deep-Sea Res. Part I Oceanogr. Res. Pap. 41, 1091–1130.

Gordon, A.L., 2005. Oceanography of the Indonesian seas and their throughflow. Oceanography 18.

Gordon, A.L., 1986. Interocean exchange of thermocline water. J. Geophys. Res. 91, 5037.

Gordon, A.L., Fine, R.A., 1996. Pathways of water between the pacific and Indian oceans in the Indonesian seas. Nature 379, 146.

Gordon, A.L., Huber, B.A., Metzger, E.J., Susanto, R.D., Hurlburt, H.E., Adi, T.R., 2012. South China Sea Throughflow impact on the Indonesian throughflow. Geophys. Res. Lett. 39.

Gordon, A.L., Susanto, R.D., 2001. Banda Sea surface-layer divergence. Ocean Dynam. 52, 2–10.

Hautala, S.L., Reid, J.L., Bray, N., 1996. The Banda for • Lausible Values of Throughflow Residence Time and Diffusivity, p. 101.

Hersbach, H., Bell, B., Berrisford, P., Hirahara, S., Horányi, A., Muñoz-Sabater, J., Nicolas, J., Peubey, C., Radu, R., Schepers, D., Simmons, A., Soci, C., Abdalla, S., Abellan, X., Balsamo, G., Bechtold, P., Biavati, G., Bidlot, J., Bonavita, M., De Chiara, G., Dahlgren, P., Dee, D., Diamantakis, M., Dragani, R., Flemming, J., Forbes, R., Fuentes, M., Geer, A., Haimberger, L., Healy, S., Hogan, R.J., Hólm, E., Janisková, M., Keeley, S., Laloyaux, P., Lopez, P., Lupu, C., Radnoti, G., de Rosnay, P., Rozum, I., Vamborg, F., Villaume, S., Thépaut, J.-N., 2020. The ERA5 global reanalysis. Q. J. R. Meteorol. Soc. 146, 1999–2049.

Hosoda, S., Ohira, T., Nakamura, T., 2008. A monthly mean dataset of global oceanic temperature and salinity derived from Argo float observations. JAMSTEC Rep. Res. Dev. 8, 47–59.

Hosoda, S., Suga, T., Shikama, N., Mizuno, K., 2009. Global surface layer salinity change detected by Argo and its implication for hydrological cycle intensification. J. Oceanogr. 65, 579–586.

Hu, D., Wu, L., Cai, W., Gupta, A. Sen, Ganachaud, A., Qiu, B., Gordon, A.L., Lin, X., Chen, Z., Hu, S., Wang, G., Wang, Q., Sprintall, J., Qu, T., Kashino, Y., Wang, F., Kessler, W.S., 2015. Pacific western boundary currents and their roles in climate. Nature 522, 299–308.

Hu, S., Sprintall, J., 2017. Observed strengthening of interbasin exchange via the Indonesian seas due to rainfall intensification. Geophys. Res. Lett. 44, 1448–1456.

Hu, S., Sprintall, J., 2016. Interannual variability of the Indonesian Throughflow: the salinity effect. J. Geophys. Res. Ocean. 121, 2596–2615.

Hu, S., Zhang, Y., Feng, M., Du, Y., Sprintall, J., Wang, F., Hu, D., Xie, Q., Chai, F., 2019. Interannual to decadal variability of upper-ocean salinity in the southern Indian Ocean and the role of the Indonesian throughflow. J. Clim. 32, 6403–6421.

Ilahude, A.G., Gordon, A.L., 1996. Thermocline stratification within the Indonesian seas. J. Geophys. Res. Ocean. 101, 12401–12409.

Katsura, S., Oka, E., Qiu, B., Schneider, N., 2013. Formation and subduction of North pacific tropical water and their interannual variability. J. Phys. Oceanogr. 43, 2400–2415.

Kessler, W.S., 1999. Interannual variability of the subsurface high salinity tongue South of the equator at 165°E. J. Phys. Oceanogr. 29, 2038–2049.

Kida, S., Richards, K.J., 2009. Seasonal sea surface temperature variability in the Indonesian Seas. J. Geophys. Res. Ocean. 114, 1–17.

Klein, S.A., Soden, B.J., Lau, N.-C., 1999. Remote sea surface temperature variations during ENSO: evidence for a tropical atmospheric bridge. J. Clim. 12, 917–932.

Koch-Larrouy, A., Lengaigne, M., Terray, P., Madec, G., Masson, S., 2010. Tidal mixing in the Indonesian Seas and its effect on the tropical climate system. Clim. Dynam. 34, 891–904.

Koch-Larrouy, A., Madec, G., Iudicone, D., Atmadipoera, A., Molcard, R., 2008. Physical processes contributing to the water mass transformation of the Indonesian throughflow. Ocean Dynam. 58, 275–288.

Lee, S.K., Park, W., Baringer, M.O., Gordon, A.L., Huber, B., Liu, Y., 2015. Pacific origin of the abrupt increase in Indian Ocean heat content during the warming hiatus. Nat. Geosci. 8, 445–449.

Li, X., Yuan, D., Li, Y., Wang, Z., Wang, J., Hu, X., Yang, Y., Corvianawatie, C., Surinati, D., Budiman, A.S., Bayhaqi, A., Avianto, P., Kusmanto, E., Santoso, P.D., Purwandana, A., Azis Ismail, M.F., Dirhamsyah Arifin, Z., 2021. Moored observations of currents and water mass properties between talaud and Halmahera islands at the entrance of the Indonesian seas. J. Phys. Oceanogr. 51, 3557–3572.

Lukas, R., 2001. Freshening of the upper thermocline in the North Pacific Subtropical Gyre associated with decadal changes of rainfall. Geophys. Res. Lett. 28, 3485–3488.

Makarim, S., Sprintall, J., Liu, Z., Yu, W., Santoso, A., Yan, X.H., Susanto, R.D., 2019. Previously unidentified Indonesian Throughflow pathways and freshening in the Indian Ocean during recent decades. Sci. Rep. 9, 1–13.

McDougall, T.J., Barker, P.M., 2011. Getting Started with TEOS-10 and the Gibbs Seawater (GSW) Oceanographic Toolbox, WG127. SCOR/IAPSO.

Metzger, E.J., Hurlburt, H.E., Xu, X., Shriver, J.F., Gordon, A.L., Sprintall, J., Susanto, R.D., van Aken, H.M., 2010. Simulated and observed circulation in the Indonesian Seas: 1/12° global HYCOM and the INSTANT observations. Dynam. Atmos. Oceans 50, 275–300.

Nakano, T., Kaneko, I., Soga, T., Tsujino, H., Yasuda, T., Ishizaki, H., Kamachi, M., 2007. Mid-depth freshening in the North Pacific subtropical gyre observed along the JMA repeat and WOCE hydrographic sections. Geophys. Res. Lett. 34.

Nakanowatari, T., Mitsudera, H., Motoi, T., Ishikawa, I., Ohshima, K.I., Wakatsuchi, M., 2015. Multidecadal-scale freshening at the salinity minimum in the western part of North Pacific: importance of wind-driven cross-gyre transport of subarctic water to the subtropical gyre. J. Phys. Oceanogr. 45, 988–1008.

Oka, E., Ishii, M., Nakano, T., Suga, T., Kouketsu, S., Miyamoto, M., Nakano, H., Qiu, B., Sugimoto, S., Takatani, Y., 2018. Fifty years of the 137°E repeat hydrographic section in the western North Pacific Ocean. J. Oceanogr. 74, 115–145.

Oka, E., Katsura, S., Inoue, H., Kojima, A., Kitamoto, M., Nakano, T., Suga, T., 2017. Long-term change and variation of salinity in the western North Pacific subtropical gyre revealed by 50-year long observations along 137$\circ$E. J. Oceanogr. 73, 479–490.

Potemra, J.T., Schneider, N., 2007. Interannual variations of the Indonesian throughflow. J. Geophys. Res. Ocean. 112, 1–13.

Redondo-Rodriguez, A., Weeks, S.J., Berkelmans, R., Hoegh-Guldberg, O., Lough, J.M., 2012. Climate variability of the great barrier reef in relation to the tropical pacific and El niño-southern oscillation. Mar. Freshw. Res. 63, 34–47.

Roemmich, D., Gilson, J., 2009. The 2004-2008 mean and annual cycle of temperature, salinity, and steric height in the global ocean from the Argo Program. Prog. Oceanogr. 82, 81–100.

Skliris, N., Zika, J.D., Nurser, G., Josey, S.A., Marsh, R., 2016. Global water cycle amplifying at less than the Clausius-Clapeyron rate. Sci. Rep. 6, 1–9.

Sloyan, B.M., Rintoul, S.R., 2001. Circulation, renewal, and modification of antarctic mode and intermediate water. J. Phys. Oceanogr. 31, 1005–1030.

Sprintall, J., Gordon, A.L., Koch-Larrouy, A., Lee, T., Potemra, J.T., Pujiana, K., Wijffels, S.E., 2014. The Indonesian seas and their role in the coupled ocean–climate system. Nat. Geosci. 7, 487–492.

Sprintall, J., Revelard, A., 2014. The Indonesian Throughflow response to Indo-Pacific climate variability. J. Geophys. Res. Ocean. 119, 1161–1175.

Sprintall, J., Wijffels, S.E., Molcard, R., Jaya, I., 2009. Direct estimates of the Indonesian throughflow entering the Indian ocean: 2004-2006. J. Geophys. Res. Ocean. 114.

Suga, T., Kato, A., Hanawa, K., 2000. North Pacific Tropical Water: its climatology and temporal changes associated with the climate regime shift in the 1970s. Prog. Oceanogr. 47, 223–256.

Susanto, R.D., Waworuntu, J.M., Prayogo, W., Setianto, A., 2021. Moored observations of current and temperature in the Alas Strait: collected for submarine tailing placement, used for calculating the Indonesian throughflow. Oceanography 34, 240–248.

Susanto, R.D., Wei, Z., Adi, T.R., Zheng, Q., Fang, G., Fan, B., Supangat, A., Agustiadi, T., Li, S., Trenggono, M., Setiawan, A., 2016. Oceanography surrounding krakatau volcano in the Sunda Strait, Indonesia. Oceanography 29, 264–272.

Talley, L.D., Baringer, M.O., 1997. Preliminary results from WOCE hydrographic sections at 80°E and 32°S in the central Indian Ocean. Geophys. Res. Lett. 24, 2789–2792.

Talley, L.D., Sprintall, J., 2005. Deep expression of the Indonesian throughflow: Indonesian intermediate water in the south equatorial current. J. Geophys. Res. C Oceans 110, 1–30.

Tan, J., Jakob, C., Rossow, W.B., Tselioudis, G., 2015. Increases in tropical rainfall driven by changes in frequency of organized deep convection. Nature 519, 451.

Tesdal, J.-E., Abernathey, R.P., Goes, J.I., Gordon, A.L., Haine, T.W.N., 2018. Salinity trends within the upper layers of the subpolar North atlantic. J. Clim. 31, 2675–2698.

Tillinger, D., Gordon, A.L., 2009. Fifty years of the Indonesian throughflow. J. Clim. 22, 6342–6355.

van Aken, H.M., Brodjonegoro, I.S., Jaya, I., 2009. The deep-water motion through the Lifamatola Passage and its contribution to the Indonesian throughflow. Deep-Sea Res. Part I Oceanogr. Res. Pap. 56, 1203–1216.

Vranes, K., Gordon, A.L., Ffield, A., 2002. The heat transport of the Indonesian Throughflow and implications for the Indian Ocean heat budget. Deep Sea Res. Part II Top. Stud. Oceanogr. 49, 1391–1410.

Wang, D., Liu, Q., Huang, R.X., Du, Y., Qu, T., 2006. Interannual variability of the South China Sea throughflow inferred from wind data and an ocean data assimilation product. Geophys. Res. Lett. 33.

Wang, J., Yuan, D., Li, X., Li, Y., Wang, Z., Hu, X., Zhao, X., Corvianawatie, C., Surinati, D., 2020. Moored observations of the Savu Strait currents in the Indonesian seas. J. Geophys. Res. Ocean. 125, e2020JC016082.

Wong, A.P.S., Bindoff, N.L., Church, J.A., 2001. Freshwater and heat changes in the north and South Pacific oceans between the 1960s and 1985?94. J. Clim. 14, 1613–1633.

Wong, A.P.S., Bindoff, N.L., Church, J.A., 1999. Large-scale freshening of intermediate waters in the Pacific and Indian oceans. Nature 400, 440–443.

Wyrtki, K., 1961. Physical Oceanography of Southeast Asian Waters. Naga Report 2.
Yao, W., Shi, J., Zhao, X., 2017. Freshening of antarctic intermediate water in the south Atlantic Ocean in 2005-2014. Ocean Sci. 13, 521–530.
Yelland, M., Taylor, P.K., 1996. Wind stress measurements from the open ocean. J. Phys. Oceanogr. 26, 541–558.
Yuan, D., Yin, X., Li, X., Corvianawatie, C., Wang, Z., Li, Y., Yang, Y., Hu, X., Wang, J., Tan, S., Surinati, D., Purwandana, A., Wardana, A.K., Ismail, M.F.A., Budiman, A.S., Bayhaqi, A., Avianto, P., Santoso, P.D., Kusmanto, E., Dirhamsyah Arifin, Z., Pratt, L.J., 2022. A Maluku Sea intermediate western boundary current connecting Pacific Ocean circulation to the Indonesian Throughflow. Nat. Commun. 13, 2093.
Yue, S., Wang, C., 2004. The mann-kendall test modified by effective sample size to detect trend in serially correlated hydrological series. Water Resour. Manag. 18, 201–218.
Zeng, L., Chassignet, E.P., Schmitt, R.W., Xu, X., Wang, D., 2018. Salinification in the south China sea since late 2012: a reversal of the freshening since the 1990s. Geophys. Res. Lett. 45, 2744–2751.
Zhang, L., Qu, T., 2014. Low-frequency variability of South pacific tropical water from Argo. Geophys. Res. Lett. 41, 2441–2446.